Editorial Manager(tm) for Acta Neuropathologica
Manuscript Draft

Manuscript Number:

Title: New ependymal cells are born postnatally in two discrete regions of the mouse brain and support ventricular enlargement in hydrocephalus

Article Type: Original Paper

Keywords: ventricular zone; radial glia; ependyma; proliferation; postnatal ependymogenesis; hydrocephalus

Corresponding Author: Dr. Luis Federico Batiz, M.D., Ph.D.

Corresponding Author's Institution: Universidad Austral de Chile

First Author: Luis Federico Batiz, M.D., Ph.D.

Order of Authors: Luis Federico Batiz, M.D., Ph.D.; Antonio Jiménez, Dr; Montserrat Guerra, Dr; Luis Manuel Rodríguez-Pérez; César D. Toledo; Karin Vio, Dr; Patricia Páez; José Manuel Pérez-Fígares; Esteban M. Rodríguez, MD, PhD

RESEARCH ARTICLE

New ependymal cells are born postnatally in two discrete regions of the mouse brain and support ventricular enlargement in hydrocephalus

Luis Federico Bátiz[1], Antonio J. Jiménez[2], Montserrat Guerra[1], Luis Manuel Rodríguez-Pérez[2], César D. Toledo[1], Karin Vio[1], Patricia Páez[2], José Manuel Pérez-Fígares[2], Esteban M. Rodríguez[1,*].

[1]Instituto de Anatomía, Histología y Patología, Facultad de Medicina, Universidad Austral de Chile, Valdivia, Chile

[2]Departamento de Biología Celular, Genética y Fisiología, Facultad de Ciencias, Universidad de Málaga, Málaga, Spain.

Short title: Postnatal ependymogenesis and hydrocephalus

---

* Corresponding author: Esteban M. Rodríguez, Instituto de Anatomía, Histología y Patología, Facultad de Medicina, Universidad Austral de Chile, Valdivia, Chile. Phone: 56-63-293011 Fax: 56-63-221604 (e-mail: erodrigu@uach.cl)

Abstract

A heterogeneous population of ependymal cells lines the brain ventricles. The evidence about the origin and birthdates of these cell populations is scarce. Furthermore, the possibility that mature ependymal cells are born (ependymogenesis) or self-renewed (ependymal proliferation) postnatally, is controversial. The present study was designed to investigate both phenomena in wild-type (wt) and hyh hydrocephalic mutant mice at different postnatal stages. Expression of PCNA and Ki-67, incorporation of BrdU and presence of mitosis were used to assay cell proliferation in situ. In wt mice, proliferating cells were found in the ventricular zone (VZ) of two distinct regions: the dorsal walls of the third ventricle and Sylvian aqueduct (SA). Most proliferating cells were monociliated and nestin+, likely corresponding to radial glial cells. Cumulative BrdU-labelling showed that most daughter cells remained in the VZ and lost nestin-immunoreactivity, and some labelled cells were multiciliated and GLUT-1+ indicating they were ependymal cells born postnatally. Pulse BrdU-labelling and Ki-67 and β-tubulin-IV immunostaining further demonstrated the presence of proliferating multiciliated ependymal cells. In hydrocephalic mutants, the dorsal walls of the third ventricle and SA expanded enormously. Such an expansion was sustained by an increased ependymogenesis and ependymal proliferation. In brief, our data indicate that (i) birthdate of ependymal cells varies with ependymal cell lineage, (ii) in discrete regions of the brain new ependymal cells are born postnatally, (iii) increased "postnatal ependymogenesis" sustains hydrocephalic ventricular enlargement, and (iv) self-renewing proliferation of mature ependymal cells should be considered as a mechanism operating in hydrocephalus and other pathologies.

Keywords: ventricular zone; radial glia; ependyma; proliferation; postnatal ependymogenesis; hydrocephalus

INTRODUCTION

The cerebral ventricles and the central canal of the spinal cord of adult mammals are lined by a single layer of specialized glial cells: the ependymal cells [1-2]. Mature ependymal cells are multiciliated and joined together by zonula adherens and gap junctions. The knowledge on the function of the ependyma is limited and several questions remain unsolved [3]. It is assumed that it plays a role as a barrier between the cerebrospinal fluid (CSF) and the neural tissue [2,4-7] and that provides protection to the brain of potentially harmful substances [8-9], [2]. Ependymal denudation [10-11] or ciliary malfunction of ependymal cells can lead to disturbances of CSF flow and even to hydrocephalus in humans and animal models [12-17].

The evidence about the origin and birthdate of ependymal cells is scarce. Multiciliated ependymal cells appear during late stages of development. As the ventricular zone (VZ) and radial glial cells (RGCs) regress, the walls of the ventricular system become gradually lined by ciliated ependyma [18]. Spassky et al. (2005) have reported that in the mouse forebrain ependymal cells derive from RGCs and that most of them are born in E14-E16, supporting the notion that ependymogenesis is predominantly a prenatal event. In rodents, maturation of ependymal cells, including the appearance of cilia [10,19] and the expression of functional proteins such as glucose transporter-1 (GLUT-1) [20] is mainly a postnatal event. In the human and rodents maturation of ependymal cells reaches a peak at different postnatal days depending on the ventricular region [10,20-22].

In mammals, the regenerative capacity of ependyma is limited [2]. Different studies have suggested that the mammalian multiciliated ependymal cells are postmitotic or terminally differentiated [19,23]. Conversely, other reports indicate that mature ependymal cells are able to proliferate and could also act as slowly proliferating neural stem cells [24-25]. Lesions involving ventricular ependyma in adult animals have been reported to be irreversible [2,23]. However, different experimental approaches suggest that ependymal proliferation may occur after certain brain injuries [25-30]. Recently, a subventricular zone-mediated ependymal repair has been proposed [31].

In hydrocephalus, the ventricular dilatation has been correlated with some pathological changes in ependymal cells, including stretching, atrophy and focal loss [22-23,32]. Interestingly, ependymal cell proliferation has also been proposed as part of the overall tissue response in hydrocephalus [30,33-34].

The hyh (hydrocephalus with hop gait) mouse develops an autosomal recessive inherited hydrocephalus [35-36]. A point mutation in alpha-SNAP (M105I) has been identified as responsible of the hyh phenotype [37-38]. The neuropathological process in this model is characterized by a patterned and progressive neuroepithelial/ependymal denudation of the walls of the ventricular system [39]. However, some ependymal regions such as the roof of the third ventricle and the dorsal wall of the Sylvian aqueduct (SA) are resistant to denudation [40-41] despite the fact that these two cavities expand enormously as hydrocephalus progresses. Since the thin walls of these expanded cavities are lined by a continuous layer of ependyma the question arises: what does sustain the great enlargement of the dorsal wall of the third ventricle and SA of the hydrocephalic mice without ependymal disruption? The hypothesis is that the several folds increase of a ventricular surface lacking discontinuities or ventriculostomies [see [40]] can only be explained by the proliferation of the cells forming the expanding walls. The aim of present study was to test this hypothesis. We explored the mitotic activity in the VZ of wild type and hyh mice during postnatal development and determined the phenotype of the proliferative cells. In addition, using 5-bromo-2'-deoxy-uridine (BrdU) we found that new ependymal cells originate postnatally in wild type mice and that this phenomenon increases dramatically in the dilated ventricles of hydrocephalic animals.

MATERIALS AND METHODS

Animals

Postnatal hyh (hydrocephalus with hop gait) mutant mice (B6C3Fe-a/a-hyh/J) were used in this study. They were obtained from the Jackson Laboratory (Bar Harbor, ME) where the hyh mutation originally arose in the C57BL/10J inbred strain and was subsequently placed on a B6C3Fe-a/a (C57BL/6J female X C3HeB/FeJ-a/a male) hybrid background [35]. These animals were bred into a colony and eight different maternal sub-lines were developed [40]. Housing, handling, care, and processing of the animals were carried out in accordance with European and Spanish laws (DC 86/609/CEE and RD 1201/2005) and following the regulations approved by the council of the American Physiological Society. All animals (hyh mutants and their wild type littermates) were genotyped by a PCR-based method according to [42].

Light Microscopy

Mice were anesthetized by intraperitoneal (i.p.) administration of 0.2 mg/g body weight of sodium pentobarbital (Dolethal; Vétoquinol, Lure, France) and perfused transcardially with Bouin fixative or 4% paraformaldehyde in 0.1M phosphate buffer, pH 7.2. The brains were removed, post-fixed in the same solutions during 24-48 h and then processed to obtain sections. Bouin-fixed samples were paraffin-embedded to obtain 8-µm-thick sections. Paraformaldehyde-fixed material was cryoprotected in 30% sucrose and frozen sections (40 µm thickness) were obtained. Paraffin sections were processed for haematoxylin-eosin staining, immunocytochemistry or immunofluorescence. Frozen sections were processed for immunofluorescence.

Immunocytochemistry

Brain samples of at least 6 animals per age (3 wt and 3 hyh) were processed for light microscopy immunocytochemistry as described previously [10,39]. Basically, samples were sequentially incubated in (i) primary antibody for 18 hours at room temperature (RT); (ii) a biotinylated secondary antibody (Vector Laboratories, Burlingame, CA) for 30 minutes at RT; and (iii) Vectastain Elite ABC reagent

(Vector Laboratories) for 30 minutes at RT. Finally, the reaction product was detected using diaminobenzidine (DAB) (Sigma, St. Louis, MO). The primary antibodies used were: mouse anti-proliferating cell nuclear antigen (PCNA) antibody (1:500; Sigma, St. Louis, MO), mouse anti-BrdU (1:50; G3G4; DSHB, Iowa City, IA) and rabbit anti-glucose transporter-1 (GLUT-1) (1:1000; kindly provided by Coralia Rivas, Universidad de Concepción, Chile). All antibodies were diluted in Tris buffer, pH 7.8, containing 0.7% non-gelling seaweed gelatin lambda carrageenan and 0.5% Triton-X 100 (both from Sigma, St. Louis, MO). Omission of the incubation in the primary antibody was used as a control of the immunoreaction. Some immunostained sections were counterstained with haematoxylin.

Immunofluorescence

Immunofluorescence staining was performed on paraffin and frozen sections as described previously [41]. Primary antibodies used were: (i) rabbit anti-caveolin-1 (1:200; Santa Cruz Biotech., San Diego, CA), (ii) mouse anti-β-tubulin IV (1:400; T7941; Sigma, St. Louis, MO or 1:150; Abcam, Cambridge, UK), (iii) rabbit anti-glucose transporter-1 (GLUT-1) (1:1000; kindly provided by Coralia Rivas, Universidad de Concepción, Chile), (iv) mouse anti-nestin (1:200; RAT-401; DSHB, Iowa City, IA); rabbit anti-glial fibrillary acidic protein (GFAP) (1:250; Biogenesis, Oxford, UK or 1:300; Abcam, Cambridge, UK), (v) rabbit anti-Ki67 (1:500; Abcam, Cambridge, UK), and (vi) mouse anti-BrdU (1:50; G3G4; DSHB, Iowa City, IA or 1:50; biotinylated; Abcam, Cambridge, UK). Appropriate secondary antibodies conjugated with Alexa Fluor 488, 568 or 594 (1:500 or 1:2000; Molecular Probes, Carlsbad, CA) were used. Streptavidin conjugated with Alexa fluor 488 (1:500; Molecular Probes, Carlsbad, CA) was used when the primary antibody was biotinylated. Sections were mounted in Vectashield (Dako) and inspected with an epifluorescence microscope provided with the multidimensional acquisition software AxioVision Rel (version 4.6) of Zeiss (Germany) or confocal laser microscopy (Olympus Fluoview 1000 microscope, Universidad Austral de Chile or Leica TCS NT microscope, Universidad de Málaga, Spain). In some samples, projections in Z-axis from a stack of consecutive confocal images were obtained using ImageJ (public domain Java image processing program).

Bromodeoxyuridine Labelling

5-bromo-2'-deoxyuridine (BrdU; Sigma, St Louis, MO) was administered to wt and mutant hyh mice to label cells undergoing proliferation (BrdU is incorporated during S-phase of cell cycle). Three different protocols were applied: Protocol 1: pulse labelling-short survival. Mice were injected i.p. with a single dose of BrdU (100 mg/kg) at P4 or P6 and sacrificed 90 minutes later. Protocol 2: cumulative labelling, short survival (wt n=6, hyh n=6). Mice were injected i.p. with 3 daily doses of BrdU (100 mg/kg) on days P4 to P6 and killed at P6, 180 minutes after the last injection. Protocol 3: pulse labelling, long survival (wt n=6, hyh n=6). Mice were injected i.p. with a single dose of BrdU (100 mg/kg) at P4 or P6 and sacrificed at P30. Brains obtained with protocol 1 were fixed in paraformaldehyde 4% and processed to obtain frozen sections; those obtained with protocol 2 and 3 were fixed in Bouin and processed to obtain paraffin-embedded sections. BrdU was detected by immunocytochemistry or immunofluorescence as previously described [43]. Double-immunofluorescence combining BrdU staining with other lineage markers was used to identify the phenotype or lineage of BrdU-labelled cells.

Scanning Electron Microscopy

Wild type and hyh mutant mice at P3 (n=4), P7 (n=6) and P14 (n=7) were processed for scanning electron microscopy as previously described [10,39]. Before processing, samples were specially dissected to expose the ventricular surface of the dorsal wall of the third ventricle and the dorsal wall of the medial region of the SA (MSA).

Data Analysis

Quantitative analysis of PCNA-immunoreactive nuclei or mitotic figures (haematoxylin-eosin stained sections) was performed in mice from P1-to-P7, P14, and P30. In each stage, at least 4 wt and 4 hyh mice were analyzed. For each animal, serial sagittal sections were obtained. The most medial section and 3 paramedial sections at each side (7 sections in total) were selected for analysis. Quantification was performed using ImageJ software (National Institutes of Health, Bethesda, MD)

in 40X digital photographs that included all the regions of interest. The total number of PCNA+ cells in the ventricular zone/ependymal lining per section were counted regardless of size, shape, or staining intensity.

Differences between groups were determined using Student's t test and were considered significant when $P < 0.05$. The statistical analysis of data was made with STATISTICA 6 software (StatSoft Inc., Tulsa, OK) and the graph plots with SigmaPlot 8.0 software (SPSS Inc., Chicago, Illinois).

RESULTS

Dilation of the third ventricle and the Sylvian aqueduct of hyh mice correlates with the enlargement of the dorsal walls of both cavities

We have previously described that hyh mice present a heterogeneous neuropathological and clinical phenotype [40]. However, all hyh mutant mice develop enormous dilations of three distinct ventricular regions: (i) the caudal horns of the lateral ventricles, (ii) the third ventricle, and (iii) the medial region of the Sylvian aqueduct (MSA). Interestingly, the dorsal walls of the two latter regions have been described as areas resistant to ependymal denudation regardless of the age or severity of hydrocephalus [10,41]. From P4 onwards, the dorsal walls of the third ventricle and MSA of hydrocephalic animals became progressively thinner and were formed by a very thin sheath of nervous tissue lined by ependymal cells (Fig. 1a-d).

The analysis of the cross sectional area of third ventricle and MSA, at different postnatal stages showed that (i) they were expanded 3 to 4 times at birth and (ii) the severity of dilations increased with age (Fig. 1f, g). The increase of the ventricular area in the MSA of hyh mice was mild during the first week and became very pronounced from P7 onwards (Fig. 1g). The third ventricle started to expand earlier (P5) (Fig. 1f). These results were parallel to those of the increase in the linear ventricular surface of the dorsal wall of both cavities (Fig. 2h, i). Interestingly, both curves showed similar slopes suggesting that the enlargement of the dorsal wall supports most of the ventricular dilatation. The linear regression analysis showed that both parameters (ventricular area and dorsal wall surface) are intimately correlated in both regions (Fig. 1j, k), confirming that the increase in ventricular volume (cross sectional area) largely depends on the expansion of the dorsal wall of both cavities.

Dilated dorsal walls of the third ventricle and the Sylvian aqueduct show an increased number of ependymal cells

Several studies have described that ependymal cells are elongated or stretched in regions where ventricular walls are dilated [23,32]. In order to address the importance of this adaptative response in the dorsal walls of the third ventricle and MSA, we count the number of ependymal cells present in a segment of ventricular

lining, 200 μm long, in hyh mutant and control mice (hyh/wt ratio), at different postnatal ages (Fig. 2). Surprisingly, before P21, when the ventricular cavities were already dilated and the cross sectional area of third ventricle and MSA in hyh mice was at least 3-4 times larger than that of wt mice (Fig. 1), the number of ependymal cells per unit length (200 μm) was similar in hyh and wt mice (hyh/wt ratio not different from 1.0) (Fig. 2a, b, d). On the other hand, from P21 to P30 the number of ependymal cells per unit length in hyh mutants diminished to approximately half of that found in control animals (Fig. 2c, d). Thus, from P21 on, ependymal stretching appears to participate in the mechanism that allows great expansion of the ventricular walls without ependymal denudation or openings such spontaneous ventriculostomies. However, before P21 ependymal cells of the dilated third ventricle and MSA dorsal walls of hyh mice were not stretched. Conversely, the absolute number of ependymal cells was significantly increased in hyh as compared to wt mice suggesting that 'new' ependymal cells had been incorporated to the ventricular lining of the expanding cavities.

Proliferative activity in the ventricular zone continues postnatally in two distinct and discrete regions of the dorsal walls of the third ventricle and the Sylvian aqueduct

In order to address whether 'new' ependymal cells were being generated during postnatal life, we first studied the proliferative activity in the dorsal walls of the third ventricle and the MSA, in wt and hyh mice. The proliferative cell nuclear antigen (PCNA) is a cofactor of DNA polymerase expressed during the S-phase of cell cycle and it has been proposed to assay cell proliferation in situ [44]. A series of brain sagittal sections immunostained using anti-PCNA at different postnatal stages (from P1 to P30) revealed that in two discrete but distinct regions of the ventricular zone (VZ) the cells continue to proliferate after birth. Indeed, PCNA+ cells were found in the VZ (ependymal lining) of the pineal recess and the habenular commissure of the third ventricle (Fig. 3a), and in the dorsal wall of the most caudal region of MSA (Fig. 3b). Interestingly, some PCNA+ cells were also found in the subependymal zone of both regions. On the other hand, no PCNA+ cells were found in the ventral wall of SA (Fig. 3a, b).

When we analyzed the same phenomenon in hyh mutant mice we found a dramatic increase in the proliferative activity at both regions (Fig. 3c-h). In MSA, the number of PCNA+ cells in the ventricular zone of hyh mice was 2-3 times higher than that of the corresponding controls, at all postnatal stages studied (Fig. 3d, h). Similar results were observed at the dorsal wall of the third ventricle (Fig. 3c, g). Worth noticing is that the location of PCNA+ cells in hyh mice was similar to that of wt mice. Indeed, the analysis of the medial-to-lateral relative distribution of PCNA+ cells in the MSA and dorsal third ventricle showed no differences between hyh and wild type mice (Fig. 3f). Furthermore, the temporal pattern of proliferative activity was similar in hyh mutant mice and wild type mice (Fig. 3g, h). The highest number of PCNA+ cells in the dorsal wall of MSA was achieved during the first 4 postnatal days in both mutant and wild type animals (Fig. 3h). In the dorsal wall of the third ventricle, the peak of PCNA+ cells was reached during the second half of the first postnatal week in both animal groups (Fig. 3g).

To confirm the presence of proliferative cells in the ventricular zone of the third ventricle and MSA we analyzed the presence of mitotic figures in both regions. No mitotic figures were identified in the ventral walls regardless of the age of the animals. Mitoses were found only in the dorsal walls of third ventricle and MSA of wt and hyh mice, which are the same zones where PCNA+ cells were found. Mitoses where significantly increased in hyh mice as compared to wt, and the temporal pattern of mitotic figures mimics that of PCNA+ cells in both regions and both conditions (Fig. 4a-f). Many of the mitotic spindles found in the ventricular zone were parallel to the ventricular surface (Fig. 4a, b, 6g).

The similarity in the regional and temporal patterns of proliferative activity (mitoses and PCNA+ cells) between mutant and control animals suggests that the higher proliferative rate observed in hyh mice is a consequence of an increase of the normal proliferative activity that occurs in wild type mice.

New ependymal cells are born postnatally in the dorsal walls of the third ventricle and the Sylvian aqueduct

The increased number of ependymal cells in the dorsal walls of the third ventricle and the MSA of hyh mice, the presence of proliferative ‘niches’ in the

ventricular zone/ependymal lining of both regions in wild type mice and the increased proliferative activity observed in mutant mice support that the enormous dilations of third ventricle and MSA is, at least in part, due to an increased postnatal ependymogenesis. In order to address the identity or phenotype of the proliferative cells and their capacity to originate ependymal cells postnatally, we combined (i) scanning electron microscopy, (ii) pulse and cumulative BrdU labelling, and (iii) double-immunolabelling for BrdU and markers of radial glial/mature ependymal cells. BrdU is a thymidine analog that incorporates to DNA of dividing cells during the S-phase of the cell cycle. BrdU is used for birth dating and monitoring cell proliferation [44].

Cumulative BrdU labelling during 72 h (P4 to P6) in wild type mice showed similar results to that obtained with anti-PCNA. Groups of BrdU-labelled cells were identified in the ventricular (ependymal) zone of the dorsal walls of the third ventricle and the MSA (Fig. 5a, b). Some BrdU+ cells were also found in the subependymal region. Interestingly, no cells were labelled in the ventral walls of both regions, confirming the results obtained with anti-PCNA and suggesting that ependymal cells of ventral walls are mainly born prenatally (Fig. 5b). Indeed, most of the ependymal cells of ventral wall of the MSA were multiciliated during the first postnatal days (Fig. 5b). Double-immunostaining for BrdU and nestin (marker of neural precursor/radial glial cells) showed that some of the BrdU+ cells of the third ventricle and most of the BrdU+ cells of the MSA were strongly immunoreactive to nestin, likely corresponding to radial glial cells (Fig. 5c, d, g). Indeed, radial basal processes were recognized in most of the nestin+ cells (Fig. 5c-e). Interestingly, many of the BrdU+ cells of the third ventricle were lightly or no immunoreactive to nestin, probably corresponding to different maturation states of the ependymal lineage (Fig. 5c-e). Scanning electron microscopy confirmed the abundance of neural progenitors/radial glial/immature ependymal cells in both regions characterized by the presence of a single cilium (Fig. 5i-l). Multiciliated mature ependymal cells were also found in both regions (Fig. 5j, l). Pulse BrdU-labelling/short survival (30 min) confirmed that most of the BrdU+ cells corresponded to monociliated progenitor cells (Fig. 5n) expressing nestin (Fig. 5g) and βtubulin IV (Fig. 5h) but not GFAP (Fig. 5o). When the same strategy was applied but with a long survival period, we found

that some of the BrdU+ cells were multiciliated and expressed GLUT-1, both considered markers of mature ependymal cells. Interestingly, in cumulative BrdU labelling, we were able to identify BrdU+/GLUT-1+ cells that were not yet multiciliated (Fig. 5m). Together, these results indicate that some ependymal cells are postnatally born and were likely derived from monociliated/nestin+ radial glial/precursor cells. Furthermore, GLUT-1 overexpression appears to precede ciliogenesis in the differentiation/maturation process of some ependymal cells.

In hyh mice, the dorsal walls of the third ventricle and MSA were lined by monociliated and multiciliated cells (Fig. 6a-c, 7a-c) resembling the appearance of the ventricular surface of wt mice (compare Fig. 6c and 5j). Pulse BrdU-labelling showed that most of the cells incorporating BrdU were monociliated (Fig. 6d, e, 7g). Cumulative BrdU labelling (P4 to P6) confirmed the results obtained with anti-PCNA, showing a dramatic increase in the number of BrdU-labelled cells. Furthermore, most of the BrdU-labelled cells remained in the ventricular (ependymal) zone (Fig. 6f; 7d). Indeed, most of the mitotic spindles found in the ventricular zone were parallel to the ventricular surface, likely originating daughter cells that would remain in the ventricular zone (Fig. 6g). Supporting this hypothesis, we found several pairs of BrdU-labelled nuclei within the ependymal lining in both regions (Fig. 7f). Similar to the wild type mice, BrdU+ cells were not immunoreactive to GFAP (Fig. 7h). As in wt mice, increased postnatal ependymogenesis in hyh mice was confirmed by the presence of many multiciliated/BrdU+ cells in pulse BrdU labelling/long survival experiments (Fig.7m) and some BrdU+/GLUT-1+ cells in cumulative BrdU labelling experiments (Fig. 7j, k).

Surprisingly, the analysis by confocal microscopy of brain samples from wild type mice subjected to pulse BrdU-labelling/short survival showed that, even though most of the BrdU+ cells were monociliated (Fig. 5), some BrdU+ cells appear to be mature, multiciliated ependymal cells (Fig. 8a, b), suggesting that some mature ependymocytes were proliferating cells. To address this possibility, serial sagittal sections through the third ventricle and the MSA were double-immunostained for both Ki67, a protein strictly associated with cell proliferation [45], and β-tubulin IV (cilia marker). Interestingly, some multiciliated cells were immunoreactive to Ki67 (Fig. 8c) and these cells were mainly found in the midline sections. The number of

proliferating ependymal cells was increased in hydrocephalic hyh mice. The analysis of confocal images in the Z-axis confirmed that Ki-67+ cells were indeed multiciliated (Fig. 8d, e)

DISCUSSION

Early evidence supports the existence of highly specialized ependymal areas distributed throughout the ventricular system [46-49]. Recently, the use of specific probes has led to the identification of several ependymal cell lineages in the SA of mouse [10,20] and human (Sival et al.2010; submitted manuscript) and in the third ventricle [50]. Many of these types of ependyma are multiciliated; therefore multiciliated ependyma should not be regarded as a homogeneous cell population but as a group of different cell lineages distributed throughout discrete regions of the ventricular walls. Surprisingly, most authors working in the field have overlooked this complexity of ependyma. Within the scope of the present investigation the question whether the different ependymal subpopulations are born at different times of development should be discussed.

Some ependymal cells are born postnatally from monociliated nestin+ cells in discrete regions of the brain ventricular walls

In mammals, it is well established that, during brain development, radial glial cells (RGCs) residing in the ventricular zone (VZ) give rise directly or indirectly to most of the neurons and astrocytes that populate the central nervous system [51-53]. In contrast, the origin of ependymal cells has not yet been fully elucidated. In mammals RGCs are also capable to originate multiciliated ependymal cells [54]. In newborn mice most cells in the VZ of the lateral wall of the lateral ventricles are RGCs and some immature ependymal cells are already present. At P7, the proportion of RGCs decreases while that of immature ependyma increases; at P15-P30 RGCs are absent from the VZ, which has been replaced ependyma [55]. The evidence suggests that in mice multiciliated ependymal cells originate from a gradual transformation of RGCs occurring mainly at early postnatal stages. A BrdU-labelling experiment has shown that most ependymal cells of the lateral ventricles are born between E14 and E16 [19]. These authors described in the ependyma of the lateral ventricles a lag of approximately 3 to 6 days between final cell division (E14-E16) and the appearance of cilia (P0-P4), which is considered a hallmark of ependymal cell differentiation or maturation. The development of cilia or ciliogenesis is also a postnatal event in SA of hyh mice [10]. Overexpression of the glucose transporter 1 (GLUT-1) in the VZ of

the mouse SA occurs during early postnatal life and follows a temporal and regional pattern that has been associated to ependymal cell differentiation [20].

Our findings suggest that certain subpopulations of ependymocytes originate during prenatal stages while others do during postnatal life. In neither of the protocols used in the present investigation (postnatal administration of BrdU, presence of PCNA+ cells or mitosis at several postnatal ages) we found signs of proliferative activity in the VZ of the lateral ventricles or in the ventral walls of SA. However, in the VZ of the dorsal wall of the third ventricle and the dorsal wall of the SA, proliferative activity and the production of a relatively large number of cells continue for at least 3 to 4 weeks after birth. Most of the proliferating cells were monociliated and nestin+, likely corresponding to RGCs. Interestingly, most of the mitotic divisions were symmetric (plane of cleavage perpendicular to the ventricular surface) indicating that a large proportion of daughter cells of dividing cells remain in the VZ. Furthermore, the presence in the VZ of BrdU-labelled cells that were monociliated and lightly or no immunoreactive to nestin, suggests gradual transformation of RGCs into ependymal cells. The existence in the third ventricle and SA of ependymal cells originated postnatally was confirmed by the presence of (i) BrdU-labelled cells that were multiciliated in pulse-labelling/long survival experiments; (ii) GLUT-1+ cells that were labelled after cumulative BrdU-labelling. The fact that some BrdU-labelled cells are GLUT-1+ but are not multiciliated after cumulative BrdU-labelling, suggest that GLUT-1 overexpression could precede the appearance of cilia in the maturation process of ependymal cells.

In brief, our results sustain the notion that most ependymal cells are derived from RGCs, do not support the generalized idea that virtually all ependymal cells are born during embryonic life rather, the present findings show that specific populations of ependymal cells are born postnatally. In this context, the existence of several subpopulations distributed throughout the ventricular walls must be kept in mind. Most of the investigations concluding that no or very few ependymal cells are born postnatally have been performed in the walls of the lateral ventricles [6,19,21-22]. Conversely, our findings suggest that there are some discrete proliferating niches in the VZ of the dorsal walls of the third ventricle and SA where ependymogenesis could take place postnatally. This view is in agreement with findings by [56] who

reported the presence of scarce nestin+ proliferative cells in the VZ of the third ventricle and SA of adult rats.

Proliferation of mature ependymal cells may contribute to postnatal ependymogenesis

The proliferative and regenerative capacity of mature ependymal cells lining the central canal of the spinal cord in response to spinal cord injury have been demonstrated in lower vertebrates [57-58] and mammals [59-60]. However, the proliferative capability of mature ependymal cells lining the brain ventricles remains controversial [18,22]. While some investigators suggest that mature ependymal cells can proliferate [1-2,24], others indicate that ependymal cells are postmitotic and do not divide after differentiation [19,23]. The administration to mice and rats, at several postnatal intervals, of [^{3}H]thymidine or BrdU led to the conclusion that ependymal cells lining the walls of the lateral ventricles do not proliferate after birth [19,61] and present study). However, we did find proliferating ependymal cells in the dorsal walls of the third ventricle and SA. Using pulse BrdU-labelling during 90 minutes we found that this S-phase marker was incorporated not only by several VZ monociliated cells but also by some multiciliated ependymal cells. Considering that BrdU labels only S-phase of the cell cycle [44], that the maturation process (ciliogenesis) of ependymal cells takes much more than 90 minutes, it seem unlikely that these multiciliated BrdU+ cells have resulted from the proliferation of monociliated VZ cells; rather, they would correspond to multiciliated ependymal cells that will undergo mitosis. The possibility that some multiciliated ependymal cells are capable to proliferate under normal conditions is further supported by the presence in the two ependymogenic niches of multiciliated ependymal cells carrying a Ki-67+ nucleus. Indeed, Ki-67 protein is strictly associated with cell proliferation, is expressed in all phases of the cell cycle and is absent from resting cells (G0), it is regarded as an excellent marker of the growth fraction of a given cell population [44-45]. The findings discussed suggest that the ependyma is not 100% post mitotic.

Under pathological conditions, [23] has suggested that human ependymal cells do not undergo mitotic proliferation. In contrast, several authors have described proliferation of ependymal cells as a response to different type of injuries [25-30].

Our observations are in agreement with these reports and suggest that dividing ependymal cells not only are present in the normal mouse brain but also dramatically increased in number under hydrocephalus.

Postnatal ependymogenesis is enhanced in hydrocephalic hyh mice

The dorsolateral wall of the lateral ventricles has an ependymogenic potential activated during aging or after neuraminidase-induced ependymal denudation [31]. Such a repair is supported by subventricular zone (SVZ) astrocytes and is associated only with ependyma with an adjacent SVZ [31]. In hyh mice, the dorsal walls of the third ventricle and SA are virtually devoid of SVZ; the hydrocephalic ventricular enlargement of these two regions is sustained by an increased postnatal ependymogenesis resulting from proliferation of RGCs and multiciliated ependymal cells. This may explain that in the expanding walls of the third ventricle and SA ependymal stretching, disruption or ventriculostomies do not occur. The molecular mechanism that triggers the increased postnatal ependymogenesis in hydrocephalic hyh mice is unknown. However, the phenotype, the distinct regional location of dividing cells and the temporal variation of mitotic activity in hydrocephalic animals mimic that of wild type mice, suggesting that this phenomenon corresponds to an enhancement of the process occurring in control mice.

The microenvironment of CSF-contacting cells is clearly influenced by the composition of the CSF. The CSF contains several compounds that could influence the proliferative/differentiation process [62-66]. The flow and composition of CSF is altered in hydrocephalus [67-68]. The level of some growth factors appears to be higher in the CSF from hydrocephalic patients or mutant animals compared to controls [69]. In this context, the role of hydrocephalic CSF on the physiology of postnatal RGCs should be studied more deeply. Cerebral isquemia, metabolic disturbances and/or mechanical injury associated to hydrocephalus [70] could also be involved in the enhancement of ependymal proliferation found in the hydrocephalic mice.

The fact that the dorsal walls of the third ventricle and SA showed proliferative capability, but the ventral walls of the same cavities did not, supports the heterogeneity of the ependymal lining and indicates that the behaviour of ependymal

cells of SA of hyh mice depends on their lineage: the ventral ependyma detaches [10], the dorsal ependyma proliferates, while the rostral ependyma neither detaches nor proliferates. Since all these ependymal sub-populations harbour the same hyh mutation and are exposed to the same environment, their differential response to the hydrocephalic status can best be explained by their distinct genetic program.

Based on the present findings, we propose that although one of the most accepted mechanisms of ependymal reaction to ventricular enlargement is the elongation or stretching of the ependymal cells [23,32], postnatal ependymogenesis and ependymal cell proliferation should also be considered as adaptative mechanisms operating in hydrocephalus.

ACKNOWLEDGEMENTS

The authors are grateful to Mr. Genaro Alvial for a reliable technical support. This work was supported by Grants from Fondecyt 1070241, Chile to EMR; Fondecyt 11090373, Chile to LFB; FIS, PI 030756 and PI 060243, Instituto de Salud Carlos III and Servicio Andaluz de Salud, Spain to JMP-F; PCI2006-A/-0669 to AJJ.

REFERENCES

1. Bruni JE, Del Bigio MR, Clattenburg RE (1985) Ependyma: normal and pathological. A review of the literature. Brain Res 356: 1-19.
2. Del Bigio MR (1995) The ependyma: a protective barrier between brain and cerebrospinal fluid. Glia 14: 1-13.
3. Sevc J, Daxnerova Z, Hanova V, Koval J Novel observations on the origin of ependymal cells in the ventricular zone of the rat spinal cord. Acta Histochem.
4. Millhouse OE (1972) Light and electron microscopic studies of the ventricular wall. Z Zellforsch Mikrosk Anat 127: 149-174.
5. Mitro A, Lojda Z (1988) Histochemistry of proteases in ependyma, choroid plexus and leptomeninges. Histochemistry 88: 645-646.
6. Sarnat HB (1992) Role of human fetal ependyma. Pediatr Neurol 8: 163-178.
7. Prothmann C, Wellard J, Berger J, Hamprecht B, Verleysdonk S (2001) Primary cultures as a model for studying ependymal functions: glycogen metabolism in ependymal cells. Brain Res 920: 74-83.
8. Carder PJ, Hume R, Fryer AA et al. (1990) Glutathione S-transferase in human brain. Neuropathol Appl Neurobiol 16: 293-303.
9. Kuchler S, Graff MN, Gobaille S et al. (1994) Mannose dependent tightening of the rat ependymal cell barrier. In vivo and in vitro study using neoglycoproteins. Neurochem Int 24: 43-55.
10. Wagner C, Batiz LF, Rodriguez S et al. (2003) Cellular mechanisms involved in the stenosis and obliteration of the cerebral aqueduct of hyh mutant mice developing congenital hydrocephalus. J Neuropathol Exp Neurol 62: 1019-1040.
11. Dominguez-Pinos MD, Paez P et al. (2005) Ependymal denudation and alterations of the subventricular zone occur in human fetuses with a moderate communicating hydrocephalus. J Neuropathol Exp Neurol 64: 595-604.
12. De Santi MM, Magni A, Valletta EA, Gardi C, Lungarella G (1990) Hydrocephalus, bronchiectasis, and ciliary aplasia. Arch Dis Child 65: 543-544.
13. Kobayashi Y, Watanabe M, Okada Y et al. (2002) Hydrocephalus, situs inversus, chronic sinusitis, and male infertility in DNA polymerase lambda-deficient mice: possible implication for the pathogenesis of immotile cilia syndrome. Mol Cell Biol 22: 2769-2776.
14. Ibanez-Tallon I, Pagenstecher A, Fliegauf M et al. (2004) Dysfunction of axonemal dynein heavy chain Mdnah5 inhibits ependymal flow and reveals a novel mechanism for hydrocephalus formation. Hum Mol Genet 13: 2133-2141.
15. Banizs B, Pike MM, Millican CL et al. (2005) Dysfunctional cilia lead to altered ependyma and choroid plexus function, and result in the formation of hydrocephalus. Development 132: 5329-5339.
16. Town T, Breunig JJ, Sarkisian MR et al. (2008) The stumpy gene is required for mammalian ciliogenesis. Proc Natl Acad Sci U S A 105: 2853-2858.
17. Wodarczyk C, Rowe I, Chiaravalli M et al. (2009) A novel mouse model reveals that polycystin-1 deficiency in ependyma and choroid plexus results in dysfunctional cilia and hydrocephalus. PLoS One 4: e7137.

18. Del Bigio MR Ependymal cells: biology and pathology. Acta Neuropathol 119: 55-73.
19. Spassky N, Merkle FT, Flames N et al. (2005) Adult ependymal cells are postmitotic and are derived from radial glial cells during embryogenesis. J Neurosci 25: 10-18.
20. Silva-Alvarez C, Carrasco M, Balmaceda-Aguilera C et al. (2005) Ependymal cell differentiation and GLUT1 expression is a synchronous process in the ventricular wall. Neurochem Res 30: 1227-1236.
21. Sarnat HB (1992) Regional differentiation of the human fetal ependyma: immunocytochemical markers. J Neuropathol Exp Neurol 51: 58-75.
22. Bruni JE (1998) Ependymal development, proliferation, and functions: a review. Microsc Res Tech 41: 2-13.
23. Sarnat HB (1995) Ependymal reactions to injury. A review. J Neuropathol Exp Neurol 54: 1-15.
24. Johansson CB, Svensson M, Wallstedt L, Janson AM, Frisen J (1999) Neural stem cells in the adult human brain. Exp Cell Res 253: 733-736.
25. Gleason D, Fallon JH, Guerra M, Liu JC, Bryant PJ (2008) Ependymal stem cells divide asymmetrically and transfer progeny into the subventricular zone when activated by injury. Neuroscience 156: 81-88.
26. Bruni JE, Clattenburg RE, Paterson JA (1983) Ependymal cells of the rat fourth ventricle: response to injury. Scan Electron Microsc: 649-661.
27. Aikawa H, Suzuki K (1986) Ultrastructural evidence of mitotic ependymal cells in 6-aminonicotinamide-treated suckling mice. Acta Neuropathol 70: 71-74.
28. Bernstein JJ (1986) Ependyma formation in adult rat spinal cord after transplantation of fetal cerebral cortex homografts. J Neurosci Res 15: 481-490.
29. Del Bigio MR, Bruni JE (1986) Reaction of rabbit lateral periventricular tissue to shunt tubing implants. J Neurosurg 64: 932-940.
30. Del Bigio MR, Bruni JE (1988) Periventricular pathology in hydrocephalic rabbits before and after shunting. Acta Neuropathol 77: 186-195.
31. Luo J, Shook BA, Daniels SB, Conover JC (2008) Subventricular zone-mediated ependyma repair in the adult mammalian brain. J Neurosci 28: 3804-3813.
32. Page RB, Rosenstein JM, Dovey BJ, Leure-duPree AE (1979) Ependymal changes in experimental hydrocephalus. Anat Rec 194: 83-103.
33. Clark RG, Milhorat TH (1970) Experimental hydrocephalus. 3. Light microscopic findings in acute and subacute obstructive hydrocephalus in the monkey. J Neurosurg 32: 400-413.
34. Page RB (1975) Scanning electron microscopy of the ventricular system in normal and hydrocephalic rabbits. Preliminary report and atlas. J Neurosurg 42: 646-664.
35. Bronson RT, Lane PW (1990) Hydrocephalus with hop gait (hyh): a new mutation on chromosome 7 in the mouse. Brain Res Dev Brain Res 54: 131-136.
36. Perez-Figares JM, Jimenez AJ, Perez-Martin M et al. (1998) Spontaneous congenital hydrocephalus in the mutant mouse hyh. Changes in the ventricular system and the subcommissural organ. J Neuropathol Exp Neurol 57: 188-202.

37. Chae TH, Kim S, Marz KE, Hanson PI, Walsh CA (2004) The hyh mutation uncovers roles for alpha Snap in apical protein localization and control of neural cell fate. Nat Genet 36: 264-270.
38. Hong HK, Chakravarti A, Takahashi JS (2004) The gene for soluble N-ethylmaleimide sensitive factor attachment protein alpha is mutated in hydrocephaly with hop gait (hyh) mice. Proc Natl Acad Sci U S A 101: 1748-1753.
39. Jimenez AJ, Tome M, Paez P et al. (2001) A programmed ependymal denudation precedes congenital hydrocephalus in the hyh mutant mouse. J Neuropathol Exp Neurol 60: 1105-1119.
40. Batiz LF, Paez P, Jimenez AJ et al. (2006) Heterogeneous expression of hydrocephalic phenotype in the hyh mice carrying a point mutation in alpha-SNAP. Neurobiol Dis 23: 152-168.
41. Paez P, Batiz LF, Roales-Bujan R et al. (2007) Patterned neuropathologic events occurring in hyh congenital hydrocephalic mutant mice. J Neuropathol Exp Neurol 66: 1082-1092.
42. Batiz LF, Roales-Bujan R, Rodriguez-Perez LM et al. (2009) A simple PCR-based genotyping method for M105I mutation of alpha-SNAP enhances the study of early pathological changes in hyh phenotype. Mol Cell Probes 23: 281-290.
43. Jimenez AJ, Garcia-Verdugo JM, Gonzalez CA et al. (2009) Disruption of the neurogenic niche in the subventricular zone of postnatal hydrocephalic hyh mice. J Neuropathol Exp Neurol 68: 1006-1020.
44. Taupin P (2007) BrdU immunohistochemistry for studying adult neurogenesis: paradigms, pitfalls, limitations, and validation. Brain Res Rev 53: 198-214.
45. Scholzen T, Gerdes J (2000) The Ki-67 protein: from the known and the unknown. J Cell Physiol 182: 311-322.
46. Fleischhauer K (1957) [Examination of the ependyma of mesencephalon and diencephalon of the turtle (Testudo graeca).]. Z Zellforsch Mikrosk Anat 46: 729-767.
47. Paul E (1967) [On the types of ependymal cells and on their regional distribution in Rana temporaria L. With remarks on the tanycytoglia]. Z Zellforsch Mikrosk Anat 80: 461-487.
48. Höfer H (1969) Zur Anatomie der circumventrikulären Organe. In: Sterba G (ed) Zirkumventrikuläre Organe und Liquor. Jena, Fischer, pp 77-88.
49. Rodriguez EM (1976) The cerebrospinal fluid as a pathway in neuroendocrine integration. J Endocrinol 71: 407-443.
50. Rodriguez EM, Blazquez JL, Guerra M (2010) The design of barriers in the hypothalamus allows the median eminence and the arcuate nucleus to enjoy private milieus: the former opens to the portal blood and the latter to the cerebrospinal fluid. Peptides 31: 757-776.
51. Gotz M, Huttner WB (2005) The cell biology of neurogenesis. Nat Rev Mol Cell Biol 6: 777-788.
52. Merkle FT, Alvarez-Buylla A (2006) Neural stem cells in mammalian development. Curr Opin Cell Biol 18: 704-709.
53. Farkas LM, Huttner WB (2008) The cell biology of neural stem and progenitor cells and its significance for their proliferation versus differentiation during mammalian brain development. Curr Opin Cell Biol 20: 707-715.

54. Jacquet BV, Salinas-Mondragon R, Liang H et al. (2009) FoxJ1-dependent gene expression is required for differentiation of radial glia into ependymal cells and a subset of astrocytes in the postnatal brain. Development 136: 4021-4031.
55. Tramontin AD, Garcia-Verdugo JM, Lim DA, Alvarez-Buylla A (2003) Postnatal development of radial glia and the ventricular zone (VZ): a continuum of the neural stem cell compartment. Cereb Cortex 13: 580-587.
56. Chouaf-Lakhdar L, Fevre-Montange M, Brisson C et al. (2003) Proliferative activity and nestin expression in periventricular cells of the adult rat brain. Neuroreport 14: 633-636.
57. Chernoff EA (1996) Spinal cord regeneration: a phenomenon unique to urodeles? Int J Dev Biol 40: 823-831.
58. Tanaka EM, Ferretti P (2009) Considering the evolution of regeneration in the central nervous system. Nat Rev Neurosci 10: 713-723.
59. Hamilton LK, Truong MK, Bednarczyk MR, Aumont A, Fernandes KJ (2009) Cellular organization of the central canal ependymal zone, a niche of latent neural stem cells in the adult mammalian spinal cord. Neuroscience 164: 1044-1056.
60. Moreno-Manzano V, Rodriguez-Jimenez FJ, Garcia-Rosello M et al. (2009) Activated spinal cord ependymal stem cells rescue neurological function. Stem Cells 27: 733-743.
61. Imamoto K, Paterson JA, Leblond CP (1978) Radioautographic investigation of gliogenesis in the corpus callosum of young rats. I. Sequential changes in oligodendrocytes. J Comp Neurol 180: 115-128, 132-117.
62. Dattatreyamurty B, Roux E, Horbinski C et al. (2001) Cerebrospinal fluid contains biologically active bone morphogenetic protein-7. Exp Neurol 172: 273-281.
63. Hochhaus F, Koehne P, Schaper C et al. (2001) Elevated nerve growth factor and neurotrophin-3 levels in cerebrospinal fluid of children with hydrocephalus. BMC Pediatr 1: 2.
64. Lafon-Cazal M, Adjali O, Galeotti N et al. (2003) Proteomic analysis of astrocytic secretion in the mouse. Comparison with the cerebrospinal fluid proteome. J Biol Chem 278: 24438-24448.
65. Bunn RC, King WD, Winkler MK, Fowlkes JL (2005) Early developmental changes in IGF-I, IGF-II, IGF binding protein-1, and IGF binding protein-3 concentration in the cerebrospinal fluid of children. Pediatr Res 58: 89-93.
66. Redzic ZB, Preston JE, Duncan JA, Chodobski A, Szmydynger-Chodobska J (2005) The choroid plexus-cerebrospinal fluid system: from development to aging. Curr Top Dev Biol 71: 1-52.
67. Mashayekhi F, Draper CE, Bannister CM et al. (2002) Deficient cortical development in the hydrocephalic Texas (H-Tx) rat: a role for CSF. Brain 125: 1859-1874.
68. Owen-Lynch PJ, Draper CE, Mashayekhi F, Bannister CM, Miyan JA (2003) Defective cell cycle control underlies abnormal cortical development in the hydrocephalic Texas rat. Brain 126: 623-631.
69. Mashayekhi F, Salehi Z (2005) Expression of nerve growth factor in cerebrospinal fluid of congenital hydrocephalic and normal children. Eur J Neurol 12: 632-637.

70. Del Bigio MR (2001) Pathophysiologic consequences of hydrocephalus. Neurosurg Clin N Am 12: 639-649, vii.

Legends

Figure 1. *The hyh phenotype is characterized by large dilations of the third ventricle (3v) and the medial third of Sylvian aqueduct (MSA) with preservation of the ependymal lining in their dorsal walls.* a, b. Midsagittal sections through the brain of a wild type (wt) mouse (a) and a hydrocephalic hyh littermate (b) at postnatal day 5 (P5). Haematoxylin-eosin staining. Note (in red) that hyh mouse displays enormous dilatations of the 3v and the MSA. Caudal region of the SA (CSA) is obliterated and rostral region of SA (RSA) is severely stenosed. Hyh phenotype also includes agenesis of the corpus callosum (cc) (asterisk in b) and cerebellar (Ce) hypoplasia. Bars denote 500 μm. c-e. MSA of a P6 hyh mouse. Double immunostaining of the dorsal wall of MSA for caveolin-1 (green) and β-tubulin IV (red) as cilia marker. The areas framed in both rectangles (c) are shown in d and e. Mature multiciliated (full arrows) and non-ciliated (broken arrow) ependymal cells (e) line the dorsal wall of the MSA and collicular recess (cr). Bars in c, d, e denote 75 μm, 20 μm and 20 μm. Insert. Detailed magnification of e. Bar denotes 6 μm. f, g. Analysis of cross-sectional area of the 3v (d) and the MSA (e) in wild type and hyh mice at different postnatal stages. h, i. Linear length of the dorsal wall surface of the 3v (f) and the MSA (g) in wild type and hyh mice at different postnatal stages. j, k. Cross-sectional area plotted against dorsal wall surface of the 3v (h) and the MSA (i). Linear regression analysis showed that both variables are intimately correlated. 4v: fourth ventricle; cr: collicular recess; Th: thalamus.

Figure 2. *Increase in the number of ependymal cells parallels enlargement of dorsal walls of the third ventricle (3v) and the medial third of SA (MSA) during first two postnatal weeks.* a-c. Sagittal sections through the dorsal wall of MSA of a P14 wild type (wt) mouse (a), a P14 hyh mouse (b) and a P21 hyh mouse (c). Haematoxylin-eosin staining. Elongation or stretching of ependymal cells was not evident before P21. Note that mature cells are multiciliated (arrows). Bars denote 20 μm. a´-c´. Detail of the region framed by rectangles in a-c. GLUT-1 immunostaining showing that mature ependymal cells (e) are strongly immunoreactive. Bars denote 8 μm. d. Quantitative and comparative analysis of the number of ependymal cells per unit

length in the dorsal wall of the 3v and the MSA in wild type and mutant hyh mice at different postnatal ages. Data are shown as the hyh/wt ratio.

Figure 3. *Proliferative activity continues postnatally in the ventricular zone (VZ) of the dorsal walls of the third ventricle (3v) and the medial region of SA (MSA) of wild type (wt) mice and is increased in hydrocephalic hyh mice.* a-d. Midsagittal sections through the 3v and the MSA of wild type (a, b) and mutant hyh mouse (c, d) at postnatal day 6 (P6) immunostained with anti-proliferating cell nuclear antigen (PCNA). Schematic views for orientation are shown. In wt mice, several PCNA+ were identified in the VZ of the dorsal wall of the 3v (a) and the caudal region of the MSA (b). In hyh mice, a significant increase in the number of PCNA+ cells was observed in both, the dorsal walls of the 3v and the MSA (dotted arrows in b and d, respectively). Bars in a, b, c, d denote 45 µm, 70 µm, 40 µm and 70 µm, respectively. Left inset in b: Detailed magnification of area framed in b showing PCNA+ nuclei (arrow) in a discrete region of the dorsal wall of SA. Bar denotes 24 µm. Right inset: PCNA+ nuclei (arrows) in the dorsal wall of a P30 wild type mouse. Bar denotes 8 µm. Right inset in d: Detailed magnification of area framed in d showing PCNA+ nuclei (arrow) in dorsal wall of MSA. Bar denotes 20 µm. e. Section adjacent to that of d immunostained for GLUT-1. The area occupied by reactive cells (delimited by blue arrows) is similar to that occupied by PCNA+ cells. Bar denotes 95 µm. Inset: detailed magnification of GLUT-1 immunoreactive cells. f. Camera lucida drawings showing the regional distribution of PCNA+ cells in sagittal sections through the 3v and the MSA of hyh mice (P4). More lateral (L) section is darker and up, and more medial (M) section is lighter and down. Red dots represent PCNA+ cells. **f', f''.** Quantitative analysis of the medial-to-lateral relative distribution of PCNA+ cells in the 3v and MSA. Data represent mean (%) ± SEM (n=4 per condition). g, h. Quantitative analysis of the PCNA+ cells in the VZ (ependymal lining) of the dorsal walls of the 3v (g) and the MSA (h) in wild type and mutant hyh mice at different ages. Data represent mean ± SEM (n=7 sections per animal and 4 animals per condition). HC, habenular commissure; PR, pineal recess; SCO, subcommissural organ; Ce, cerebellum; 4v: fourth ventricle.

Figure 4. *Mitotic figures are seen in the ventricular zone (VZ) of the dorsal walls of the third ventricle (3v) and the medial region of SA (MSA) of wild type (wt) mice and hydrocephalic hyh mice.* a, b. Midsagittal sections through the brain of hyh mice. Haematoxylin-eosin staining. a. Dorsal wall of the third ventricle at P6. Note the presence of mitotic figures in the VZ (arrows). Pi, pineal. b. Dorsal wall of the medial region of the SA (MSA) at P14. In many cases the orientation of the plane of cell cleavage was perpendicular to the ventricular surface (dotted line). Bars denote 7 μm. c, d. Schematic drawings showing differences in the orientation of the plane of cleavage during cell division. When the plane of cleavage is parallel to the ventricular surface (asymmetric divisions) (c), one daughter cell remains in the VZ and the other is incorporated to the subventricular or subependymal zone. When the plane of cleavage is perpendicular to the ventricular surface (symmetric division) (d), both daughter cells remain in the VZ. e, f. Counting of mitotic figures in the VZ (ependymal lining) of the dorsal walls of 3v (e) and MSA (f) in wild type and mutant hyh mice at different ages. Data represent mean ± SEM (n=7 sections per animal and at least 4 animals per condition).

Figure 5. *Proliferating cells in the postnatal ventricular zone (VZ) correspond to monociliated/nestin+ cells and are capable to originate ependymal cells in wild type mice.* a-g. Midsagittal sections through the third ventricle (3v) (a, c, d-f) and the caudal region of Sylvian aqueduct (SA) (b, g) of wild type mice at P6. a, b. Immunostaining for BrdU after cumulative BrdU-labelling. Haematoxylin counterstaining. Note the presence of many BrdU-labelled cells in the VZ of the dorsal wall of both regions (arrows). No BrdU-labelled cells were found in the ventral walls. Bars denote 30 μm (a) and 22 μm (b). Inset in a: Detailed magnification of area framed in a showing BrdU-labelled ependymal cells lining the habenular commissure (arrow). Bar denotes 15 μm. Top right inset in b: Low magnification view used for orientation. Frames a and b correspond to figures a and b. Bar denotes 380 μm. Top left inset in b: detailed magnification of area framed in b showing BrdU-labelled ependymal cells in dorsal wall of SA (arrow). Bar denotes 11 μm. Bottom inset in b: Double-immunostaining for caveolin-1 (green) and β-tubulin IV (red) showing that at P6 the ventral wall of SA is lined by multiciliated/caveolin-1+ mature ependymal

cells. Bar denotes 15 μm. c-g. Double-immunostaining for nestin (red) and BrdU (green) after cumulative BrdU-labelling. c. Pineal recess region. BrdU+ cells in the VZ of the dorsal wall of 3v were strongly (d), lightly (e) or no-immunoreactive (f) to nestin. d-f. High-magnification of the regions framed in (c). Bars denote 20 μm (c) and 8 μm (d). G. Region similar to that shown in (b). Note that a discrete region of the dorsal wall of SA is strongly immunoreactive to nestin (white full arrow) but ventral wall is not (white dotted arrow). BrdU-labelled cells (yellow arrows) are nestin immunoreactive. Arrow "SEM" indicates the direction at which this region was viewed under the scanning electron microscope as shown in figure k. Bar denotes 20 μm. Inset: Detailed view of region framed in g showing a BrdU+/nestin+ cell. Bar denotes 10 μm. h. Section adjacent to that of figure g. Double-immunostaining for caveolin-1 (green) and β-tubulin IV (red) showing that in the dorsal wall of SA there are multiciliated (bottom inset) and non-multiciliated (arrow, top inset) cells. Bar denotes 40 μm. i-l. Scanning electron microscopy of the 3v (i, j) and MSA (k, l). i. Pineal recess (PR) region similar to that shown in a. Thick arrows indicates the direction at which this region was viewed under the scanning electron microscope as shown in figure j. Bar denotes 45 μm. j. Detailed view of the ventricular surface of the dorsal wall of the 3v (pineal recess) as depicted by the arrow in h. The wall is mainly lined by monociliated cells (arrows). Scarce multiciliated cells are also shown (asterisk). Bar denotes 4 μm. k. View of the dorsal wall of caudal region of the MSA as depicted by the thick arrow (SEM) in g, showing a region mostly lined by monociliated cells. The area framed is shown in l. Bar denotes 30 μm. l. Detailed view of the area framed in k mostly lined by monociliated cells (arrows) and a few multiciliated cells (asterisk). Bar denotes 4 μm. m-o. Dorsal wall of MSA of wild type P6 mice. m. Double-immunolabelling for BrdU (red) and GLUT-1 (green) after cumulative BrdU-labelling (72 h). BrdU+/GLUT-1+ cells are shown (arrow). Bar denotes 12 μm. Inset: Detailed magnification of BrdU+/GLUT-1+ cells seen in m. Bar denotes 6 μm. n. Double-immunostaining for BrdU (red) and β-tubulin IV (green) after a pulse of BrdU (90 min). Most BrdU-labelled cells are monociliated (arrow). Bar denotes 3 μm. o. Double-immunostaining for BrdU (red) and GFAP (green) after cumulative BrdU-labelling (72 h). BrdU-labelled cells (arrow) are not

GFAP immunoreactive. Bar denotes 9 µm. Ce, cerebellum; HC, habenular commissure; E, ependyma; PR, pineal recess; SCO, subcommissural organ.

Figure 6. *Postnatal ependymogenic activity increases in the dorsal wall of the third ventricle (3v) of hyh hydrocephalic mice.* a. Scanning electron microscopy of a midsagittal section through the brain of a hyh mouse at P2. Enlargement of pineal recess (PR) is already evident (compare with figure 5I). Bar denotes 100 µm. b. Scanning electron microscopy of the dorsal region of the third ventricle (3v) including the pineal recess (PR) of a mutant hyh mouse at P6. Arrow indicates the direction at which this region was viewed under the scanning electron microscope as shown in figure c. Bar denotes 100 µm. c. Ventricular surface of the roof of the 3v (pineal recess) as depicted by arrow in (b). The wall is mainly lined by monociliated cells (arrows). Scarce multiciliated cells are also shown (asterisk). Bar denotes 3 µm. d. Double-immunolabelling for BrdU (red) and β-tubulin IV (green) after pulse BrdU-labelling (90 min). Z-stacking image of confocal microscopy. View from the ventricular surface similar to that shown in (c). Note that there are monociliated (full arrow) and multiciliated (dotted arrow) cells but BrdU-labelled cells are monociliated. Bottom inset: Image of Z-axis at the level of the grey lines showing a monociliated (arrow) BrdU-labelled cell. Bar denotes 8 µm. e. Detailed view of previous figure showing a BrdU+/monociliated cell (full arrow) and a multiciliated cell (broken arrow). Bar denotes 3 µm. f. Roof of third ventricle (habenular commissure, HC) of a P6-hyh mouse treated for cumulative BrdU-labelling (72 h). Note the increase in the number of BrdU-labelled cells (compare with figure 5a). Most of BrdU+ cells remain in the ventricular zone (arrows). Bar denotes 20 µm. g. Detailed view of previous figure. Labelled mitotic spindles parallel to the ventricular surface (arrow) were found between BrdU-labelled nuclei. Bar denotes 6 µm. h. Double immunostaining for BrdU (red) and GFAP (green). BrdU+ cells of the dorsal wall of the 3v were not GFAP immunoreactive. Bar denotes 20 µm. HC, habenular commissure; PR, pineal recess; SCO, subcommissural organ.

Figure 7. *Postnatal ependymogenic activity increases in the dorsal wall of the medial third of the Sylvian aqueduct (MSA) of hyh hydrocephalic mice.* a. Scanning electron

microscopy of MSA. The area framed in lower rectangle is shown in b. An area similar to that framed by top rectangle is shown in d. Bar denotes 140 µm. b. Scanning electron microscopy of area framed in a. The denuded ventral wall of SA (V) and the dorsal wall (D) lined by ependyma are shown. White arrows indicate the border between denuded and intact walls. Double red arrows show the region of obliteration of SA. Stars indicate the obliterated region of SA. Bar denotes 24 µm. c. Detailed view of an area similar to that framed in b. Moniciliated (arrow) and multiciliated cells are intermingled. Bar denotes 4 µm. d-f. Roof of MSA. Area similar to that shown in top rectangle of figure a. BrdU immunostaining and haematoxylin counterstaining after cumulative BrdU-labelling during 72 h. d. Note the increase in the number of BrdU-labelled cells and that most BrdU+ cells remain in the ventricular zone. Bar denotes 20 µm. e. Detailed view of previous figure showing BrdU+ in the ventricular zone and at the external surface of the MSA wall (arrow). Bar denotes 15 µm. f. Pairs of BrdU+ cells, likely corresponding to daughter cells of a recent mitosis (arrows) were frequently found in the VZ. Bar denotes 8 µm. g. Double-immunolabelling for BrdU (red) and β-tubulin IV (green) after pulse BrdU-labelling (90 min) showing multiciliated cells (broken arrow) and a monociliated BrdU-labelled cell (full arrow). Bar denotes 5 µm. h, i. Double immunostaining for BrdU (red) and GFAP (green) after cumulative BrdU-labelling. (h) BrdU+ cells of the dorsal wall of MSA are not GFAP immunoreactive. Bar denotes 10 µm. i. Internal positive control. GFAP+ astrocytes cover the denuded ventral wall of the fourth ventricle (4v). Bar denotes 15 µm. j, k. Double-immunolabelling for BrdU (red) and GLUT-1 (green) in the dorsal wall of the MSA after cumulative BrdU-labelling. j. BrdU+/GLUT-1+ cells were identified at P6. Bar denotes 8 µm. Inset: Detail of cell shown in j. Bar denotes 5 µm. (k) Pair of BrdU+/GLUT-1+ cells of the dorsal wall of the MSA analyzed by confocal microscopy. Bar denotes 6 µm. l, m. Pulse BrdU-labelling/long survival experiment. Hyh mice received a single injection of BrdU at P6 and were killed at P30. Double-immunostaining for BrdU (red) and β-tubulin IV (green). l. BrdU-labelled multiciliated mature ependymal cells (i.e. ependymal cells born at P6) are shown (broken arrow). Bar denotes 4 µm. m-m'. Multichannel views of the same BrdU+

multiciliated ependymal cell. m''. Overlaid image. Bar denotes 3 μm. HC, habenular commissure; PR, pineal recess; SCO, subcommissural organ.

Figure 8. *Some mature multiciliated cells are proliferating under normal and pathological conditions.* a-c. Sagittal sections thorough the roof of third ventricle (3v) (a, b) and Sylvian aqueduct (c) of a wild type (wt) mouse at P7. a, b, b´. Double-immunolabelling for BrdU (red) and β-tubulin IV (green) after pulse BrdU-labelling (90 min). A monociliated BrdU-labelled cell (full arrow) and multiciliated BrdU-labelled cells (broken arrows) in the ventricular zone are shown. Bars denote 5 μm. c. Double-immunolabelling for Ki-67 (red) and β-tubulin IV (green). Confocal microscopy (multiple Z-planes) showing a multiciliated Ki-67+ cell (broken arrow) in the ventricular zone of the dorsal wall of SA. Bar denotes 4 μm. d, e. Sagittal sections thorough the third ventricle (3v) (d) and the medial region of Sylvian aqueduct (MSA) (e) of a hyh mouse at P4. Double immunostaining for Ki-67 (red) and β-tubulin IV (green). d, d'. Confocal microscopy of the dorsal wall of third ventricle showing a multiciliated Ki-67-labelled cell (broken arrow). Multiple Z-planes (d) and Z-axis view (d') are shown. Bar denotes 4 μm. e, e'. Confocal microscopy showing two multiciliated Ki-67+ cells in the dorsal wall of MSA (broken arrows). View from the ventricular surface of multiple Z-planes (e) and pseudo 3D images (e') are shown. Bar denotes 4 μm.

figure

Click here to download figure: figure 1 - batiz et al 2010.ppt

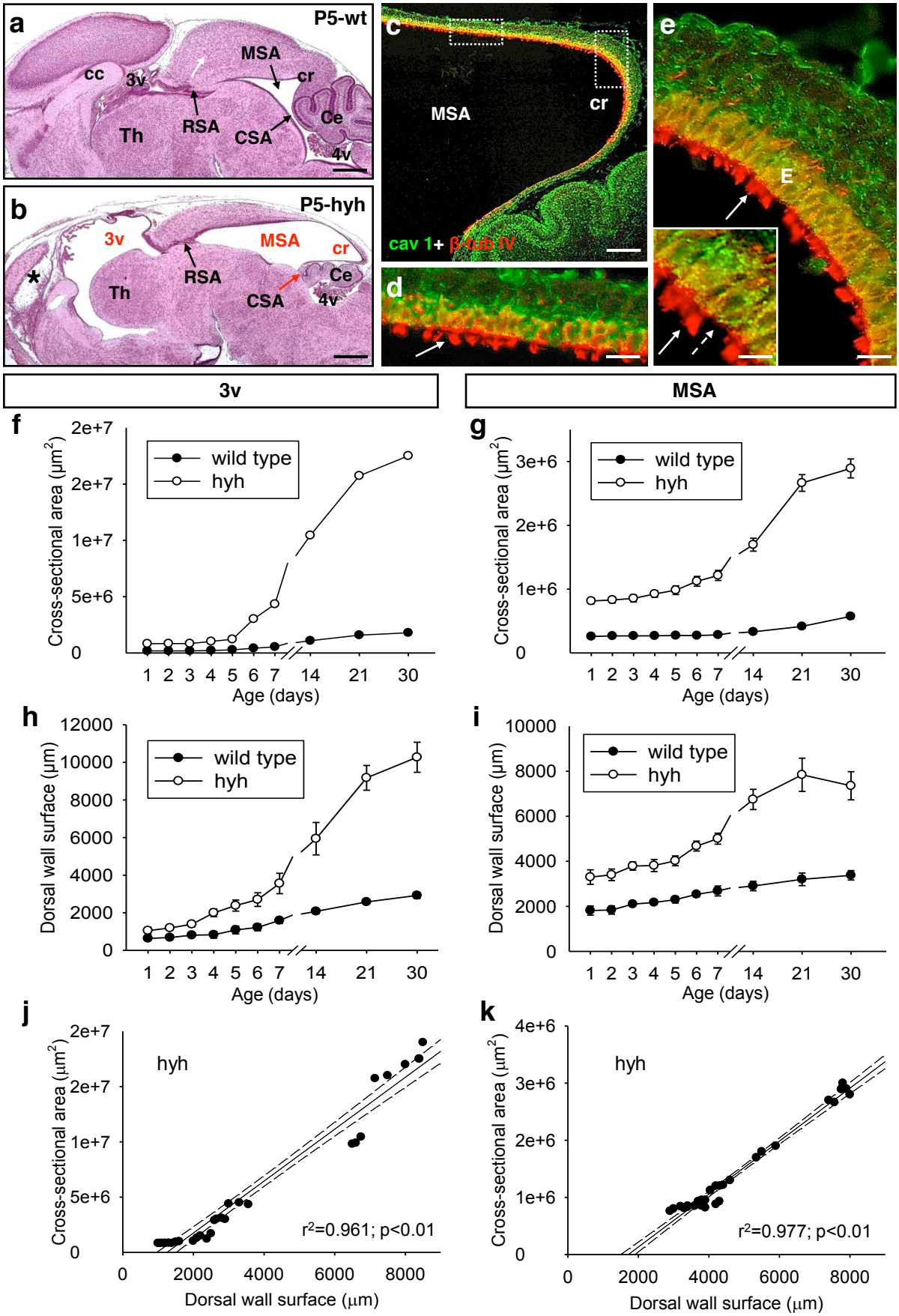

Figure 1. ***Bátiz et al. 2010***

figure
Click here to download figure: figure 2 - batiz et al 2010.ppt

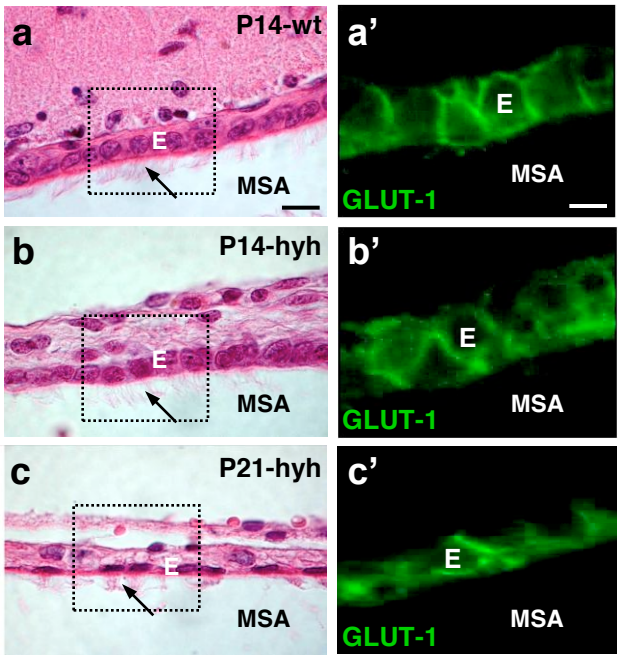

d

Age (days)	Number of ependymal cells (hyh/wt ratio) MSA (dorsal wall)	3rd ventricle (dorsal wall)
1	0,9462	0,9115
2	0,9417	0,8889
3	0,9557	0,8824
4	0,9329	0,8143
5	0,9184	0,8158
6	0,9292	0,7788
7	0,9117	0,7495
14	0,8914	0,7385
21	0,6388	0,4595
30	0,5905	0,4444

Figure 2. ***Bátiz et al. 2010***

figure

Click here to download figure: figure 3 - batiz et al 2010.ppt

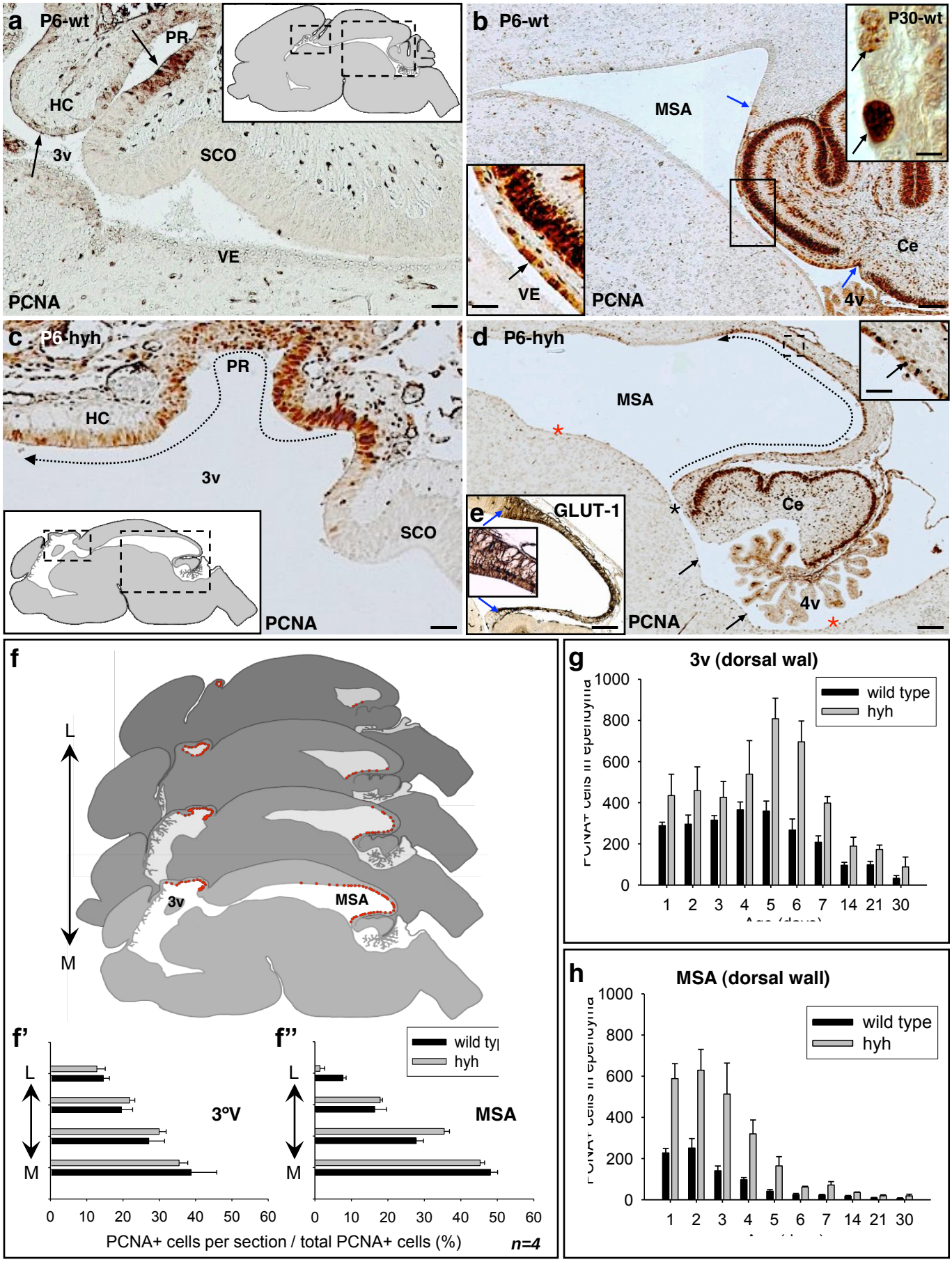

Figure 3. ***Bátiz et al. 2010***

figure
Click here to download figure: figure 4 - batiz et al 2010.ppt

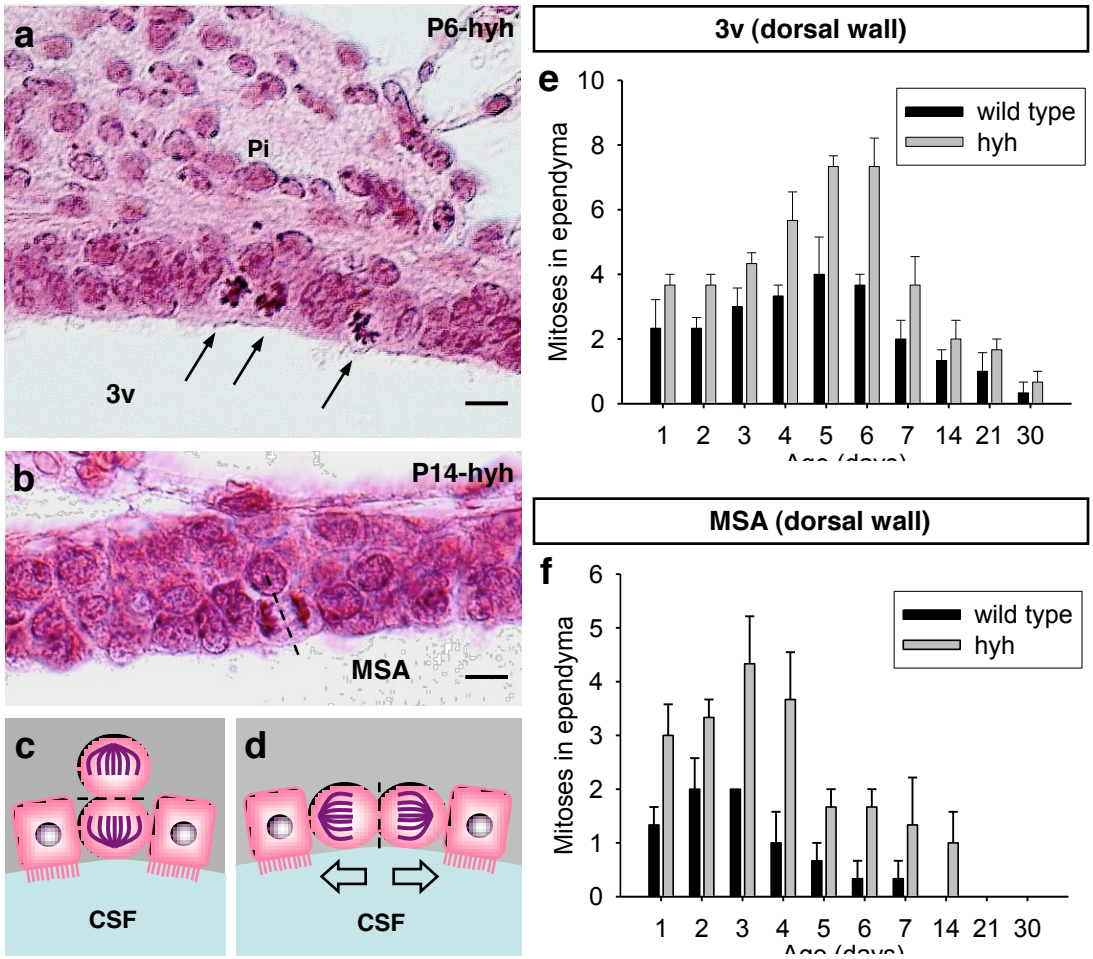

Figure 4. ***Bátiz et al. 2010***

figure

Click here to download figure: figure 5 - batiz et al 2010.ppt

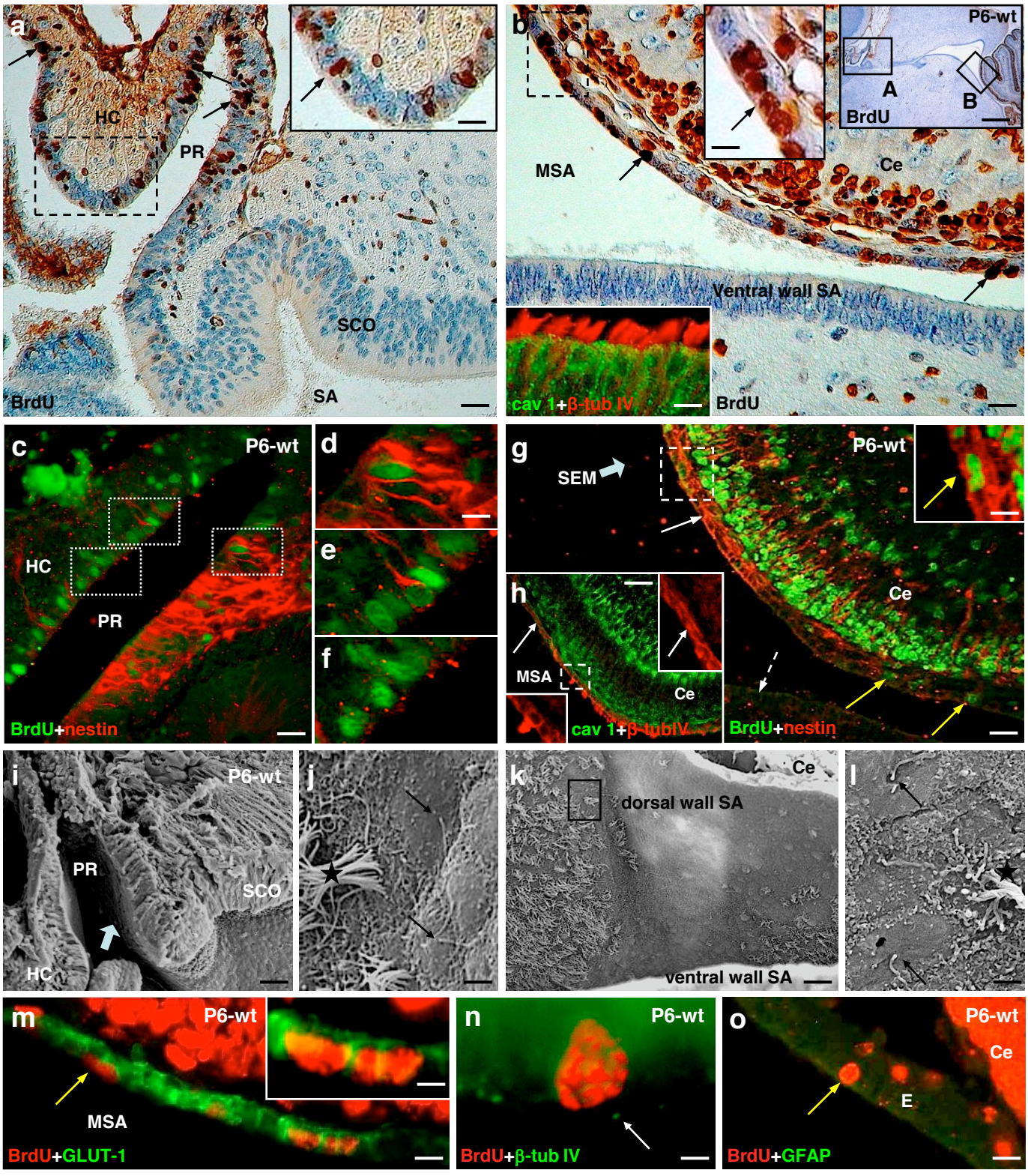

Figure 5. ***Bátiz et al. 2010***

figure
Click here to download figure: figure 6 - batiz et al 2010.ppt

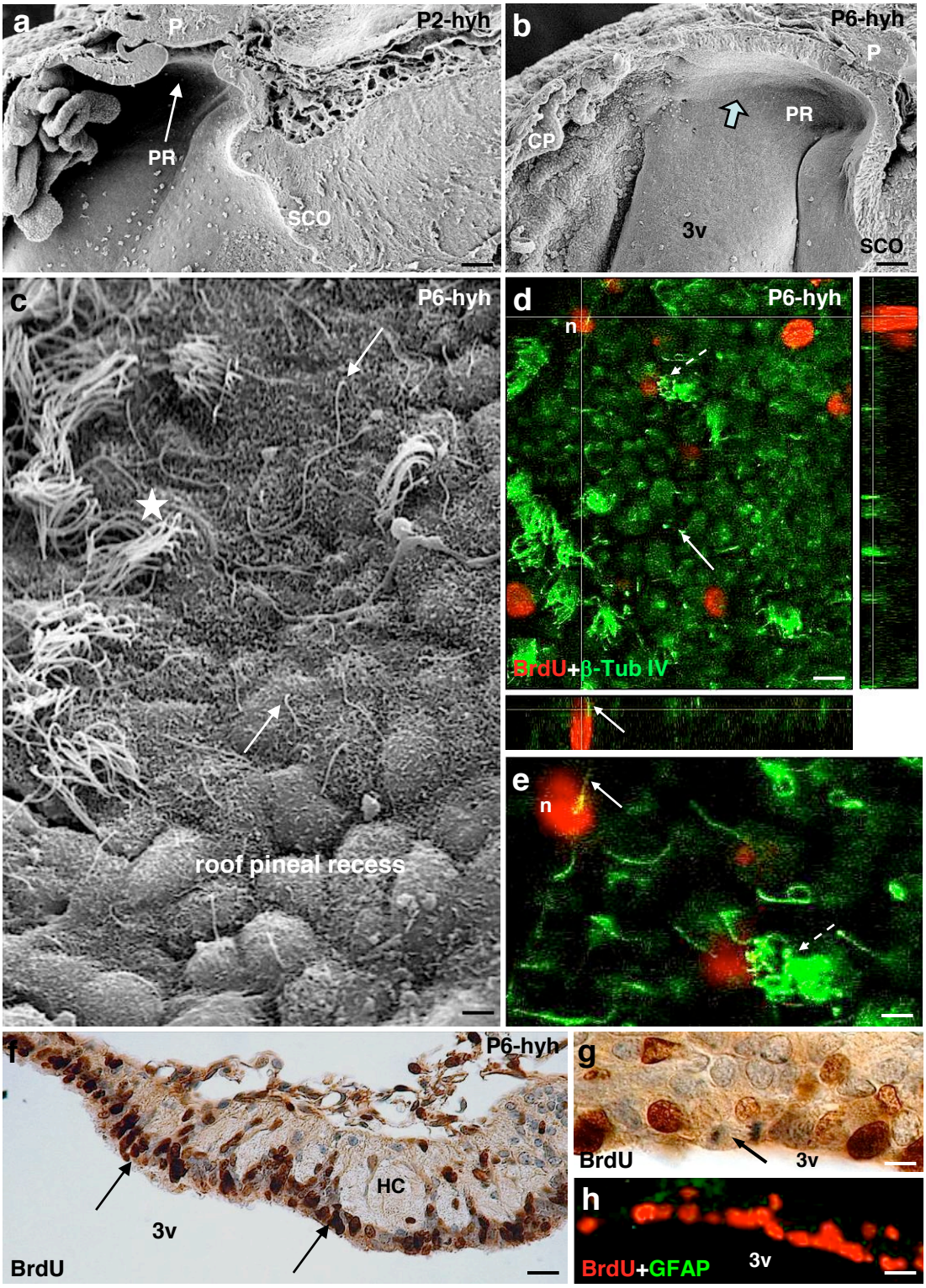

Figure 6. ***Bátiz et al. 2010***

figure
Click here to download figure: figure 7 - batiz et al 2010.ppt

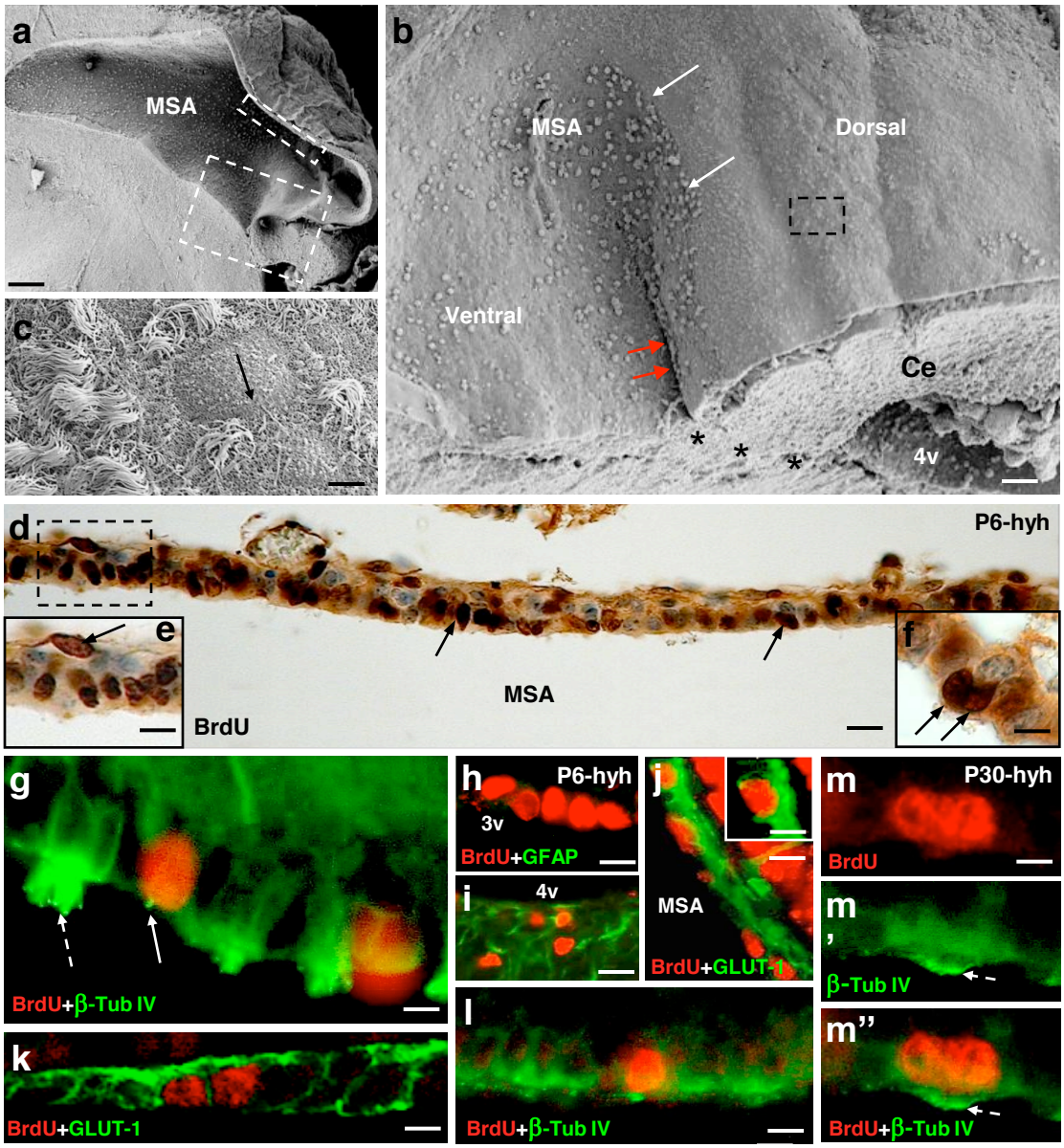

Figure 7. ***Bátiz et al. 2010***

figure
Click here to download figure: figure 8 - batiz et al 2010.ppt

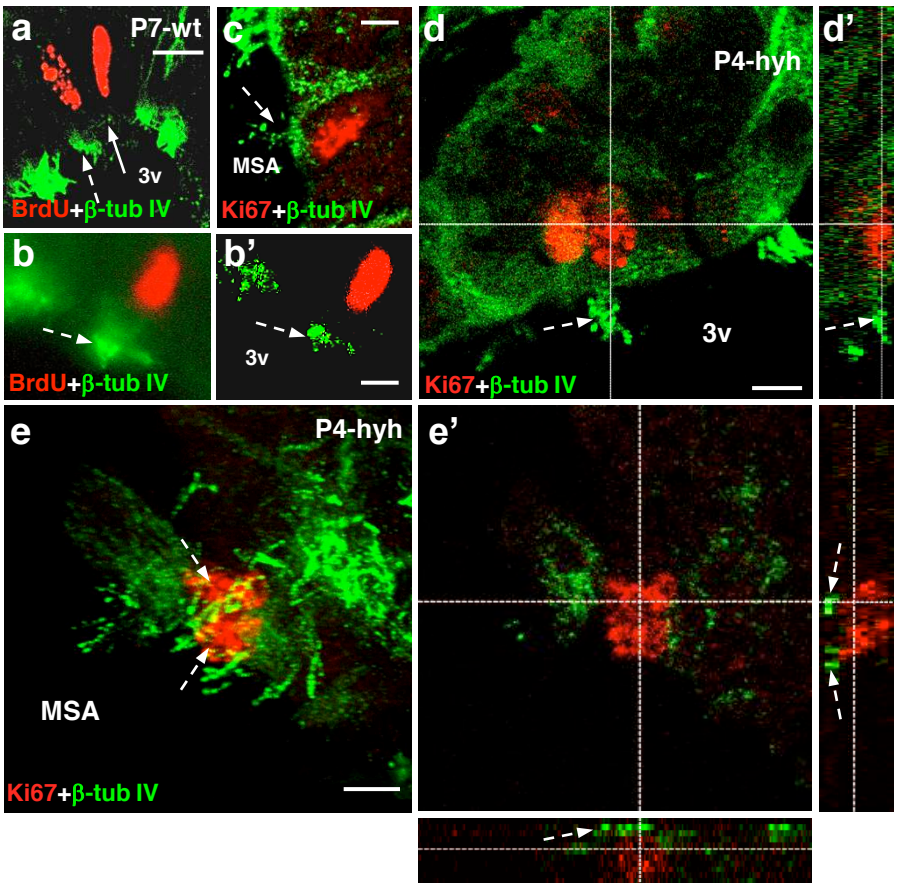

Figure 8. ***Bátiz et al. 2010***